2007 年 3 月,第 13 卷,第 1 期:75 - 88 页
March 2007, Vol. 13, No. 1, p. 75 - 88

高 校 地 质 学 报
Geological Journal of China Universities

Fault Throw Profile and Kinematics of Normal Fault: Conceptual Models and Geologic Examples

(正断层断距纵剖面图及其运动学:概念模型与地质实例)

Ge Hongxing (戈红星), Jon K. Anderson

(ConocoPhillips Company, P. O. Box 2197, Houston, TX 77252)

Abstract: Fault throw profile (T-H plot) plots vertical fault throw versus geologic or seismic horizon from a cross section. Conceptual models demonstrate that the profiles can be used to determine the styles, timing of initiation, and kinematic histories of normal faults and simply inverted normal growth faults. A throw profile comprising a vertical line segment indicates a simple postdepositional fault. A profile in which throw decreases as horizon age increases indicates a simple postdepositional keystone-stretching fault. A profile in which throw increases as horizon age increases indicates a simple growth fault. Major inflections in a composite profile correspond to the time at which fault style changes. The change of a vertical line segment to a curve with negative slope indicates the change from postdepositional to syndepositional faulting. Stacking of such composite profiles suggests repeated fault burial and rejuvenation. The change of a profile slope from positive to negative indicates change from a postdepositional keystone-stretching fault to a growth fault. The maximum throw in the profile corresponds to the start timing of the fault. Local normal drag increases apparent throw, which creates bumps in the profile. Reverse drag decreases the apparent throw, which creates dents in the profile.

Key words: normal fault; throw profile; kinematics; conceptual model; structural geology

摘要(中译文):断距纵剖面图(T-H 图)是指以断层的垂直断距为横轴、以地层或地质年龄为纵轴所绘制的随地层或地质年龄所变化的断距分布图。断距纵剖面图为确定正断层类型、断层形成时间和断层的纵向演化史提供了一个简单迅捷的工具。概念模型表明,断距纵剖面图可以明确无误地区分出简单后沉积型正断层、后沉积拱顶拉张型正断层、同沉积生长型正断层及其复合型正断层。简单后沉积型正断层的断距不随地层年龄的变化而变化,其断距纵剖面图为一垂直线段。后沉积拱顶拉张型正断层的断距随地层年龄的增大而减小并趋向零值,同沉积生长型正断层的断距随地层年龄的增大而增大,复合型正断层则具其组合型断距纵剖面形态。除简单后沉积型正断层外,断距纵剖面图中的最大断距点代表了该断层的起始形成年代。

关键词:正断层;断距纵剖面图;运动学;概念模型;构造地质学
中图分类号:P542.31　　**文献标识码**:A　　**文章编号**:1006 - 7493(2007)01 - 0075 - 14

1 Introduction

Normal faults form in all tectonic regimes in the upper crust where hydrocarbons form and accumulate. They can impact every aspect of a hydrocarbon system from source to migration to entrapment (e. g., Allan, 1989; Demaison and Huizinga, 1991; Hardman and Booth, 1991). Normal faulting can be constructive to the hydrocarbon systems. It creates accommodation space for deposition of source and reservoir sediments, provides vertical hydrocarbon migration pathways, and forms traps. Normal faulting can also be destructive.

收稿日期:2006 - 05 - 16;**修回日期**:2006 - 07 - 22

作者简介:戈红星,男,1964 年生,南京大学地质系 1985 届学士,美国科罗拉多州立大学地球资源系 1990 届硕士,美国德克萨斯大学(澳斯汀)地质系 1996 届博士,现任美国康菲公司高级地质师,主要从事盐构造地质学、拉张构造地质学及石油勘探与开发等方面的工作。Email: hongxing. ge@ conocophillips. com

Reactivation of preexisting faults and formation of new faults can weaken or destroy top and lateral seals. Faults of different ages, styles, and growth histories may have variable sealing potentials, which can affect field development planning. Different fault sets may have different response to the current stress field, which may pose significant problems for well drilling and completion.

Timing and growth history of normal faults have been estimated through analyses of regional tectonics (e. g., Davis et al, 1996), stratigraphy across the faults (e. g., Morley, 2002; Derer et al, 2003), fault displacement variations (e. g., Watterson, 1986; Barnett et al, 1987; Beach and Trayner, 1991; Chapman and Meneilly, 1991; Walsh and Watterson, 1991), and rigorous palinspastic structural reconstruction (e. g., Rowan and Kligfield, 1989; Worrall and Snelson, 1989; Nunns, 1991; Schultz-Ela, 1992).

Williams and others (1989) plotted apparent hanging wall depth versus apparent displacement (T-Z plot) to distinguish prerift, synrift, and inversion tectonostratigraphy. The plot yielded a curve with a negative slope for the growth sedimentary package and a vertical line segment for the prerift package. Bischke (1994) plotted vertical separations of horizons versus depth from wells or seismic data. In the plot, a positive slope of the curve indicated expanded sedimentary sections, a negative slope indicated condensed sections, and flat curves indicated environments free of differential tectonic movement.

This paper introduces a fault throw plot (T-H plot) technique that allows rapid assessment of style, timing of initiation, and growth history of a normal fault. The method plots fault throw measured between horizon cutoffs versus stratigraphic horizon or geologic age in outcrops, cross sections, and seismic profiles. Fault throws are used instead of displacements because throws can be readily and rapidly obtained, especially in seismic profiles. We first introduce conceptual models to illustrate throw profiles for simple and composite faults. We then investigate the influences of near-fault deformation on the shapes of the throw profiles. We finally apply our model results to nine normal faults in the Peng Lai 19-3 Oil Field in the Bohai Bay basin, offshore China, to evaluate their kinematic histories.

2 Conceptual Models

2.1 Basic Models

Fault throw profiles distinctively differentiate three basic types of normal faults: (1) simple postdepositional fault, (2) simple postdepositional crestal keystone-stretching fault, and (3) simple growth fault, which are called type I, type II, and type III fault, respectively, for cross reference. Type I fault forms after all sedimentary layers are deposited. It cuts the entire stratigraphic section with a constant throw. Type II fault also forms after all layers are deposited. It commonly forms at the crests of anticlines in response to the outer arc stretching of the bending strata. Type III fault is a syndepositional normal growth fault, where sedimentary sections expand in the hanging wall.

2.1.1 Type I fault

Figure 1a shows a schematic cross section through a type I fault. The fault formed after all the sedimentary layers 0~5 were deposited. It cut the entire prekinematic section with a constant throw during a single phase or multiple phases of extension. As a result, the T-H plot is a straight vertical line (solid line in Figure 1b). The timing of faulting post-dates the upper end point (layer 5) of the line segment in the profile.

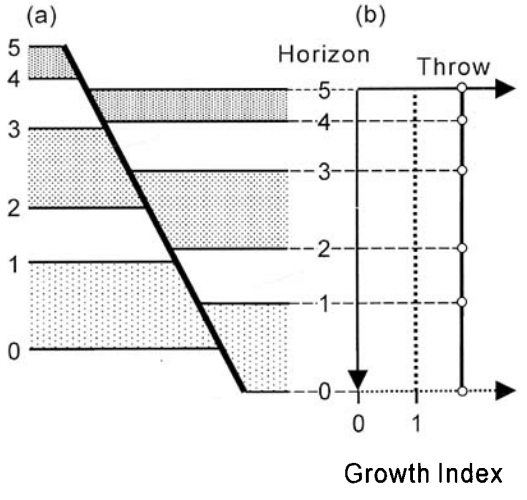

Fig. 1 (a) Schematic cross section through a simple postdepositionl normal fault and (b) T-H plot (thick solid line) and growth index plot (thick dotted cruve)

图1 (a)简单后沉稷正断层剖面示意图及其(b)断距 纵剖面图(粗实线)和断层生长指数图(粗点线)

Also plotted in Figure 1b is the fault growth index or expansion index (Tearpock and Bischke, 1991), which is 1.0 for all layers since there is no thickness

change of the equivalent strata across fault.

2.1.2 Type II fault

Figure 2a shows a schematic cross section through a type II fault. The fault is a crestal keystone-stretching fault, which formed after all the sedimentary layers 0 ~ 5 were deposited. Type II faults form at the crests of anticlines in most geologic settings. Experimental studies (e.g., Link, 1930; McClay and Ellis, 1987; Ge and Vendeville, 1994) showed that the keystone faults commonly started at the outermost layer of the stratal section, where the stretching was greatest. In the models, the faults propagated downward and increased in displacement as deformation continued. The crestal keystone faults tip out at depth.

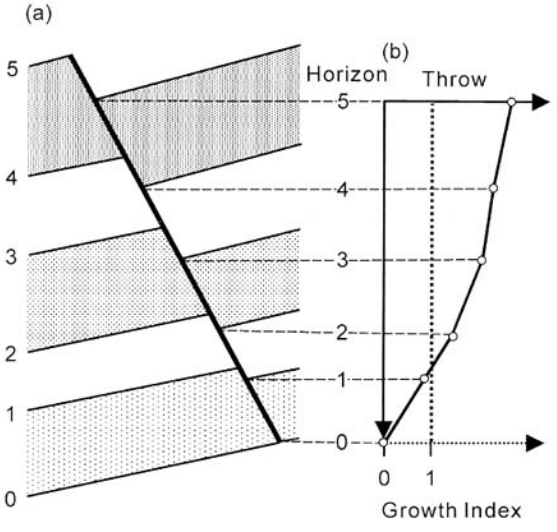

Fig. 2 (a) Schematic cross section through a postedepositional crestal keystone-strectching fault and (b) T-H plot (thick solid line) and growth index plot (thick dotted curve)

图 2 (a)后沉积拱顶拉伸正断层剖面示意图及其(b)断距纵部面图(粗实线)和断层生长指数图(粗点线)

The corresponding T-H plot is shown as a solid curve in Figure 2b. The uppermost and youngest horizon 5 has the largest throw because faulting started there and the strata was bent the most. The throw progressively decreases into the older layers at depth and is zero where the fault tips out at layer 0. The timing of fault formation post-dates the deposition of layer 5, where it records the largest fault throw.

Theoretically, the growth index (thick dotted curve in Figure 2b) should be 1.0 because sedimentary layers are pre-faulting. However, the hanging wall may be thinned by stretching, faulting, and fracturing, which results in growth index value to be smaller than 1.0. Nevertheless, the overall geometry of the growth index profile remains similar to that of type I fault: growth index plot likely cannot distinguish between type I and type II faults.

2.1.3 Type III fault

Figure 3a shows a schematic cross section through a type III fault, a simple normal growth fault. Faulting was contemporaneous with sedimentation, which resulted in expansions of sedimentary layers in the hanging wall. In the model, faulting started after layer 0 was deposited and remained active through all the sedimentation to layer 5.

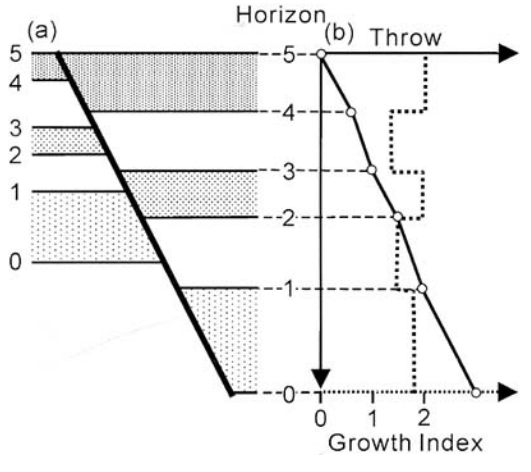

Fig. 3 (a) Schematic cross section through a simple normal growth fault and (b) T-H plot (thick solid line) and growth index plot (thick dotted curve)

图 3 (a)简单生长正断层剖面示意图及其(b)断距纵部面图(粗实线)和断层生长指数图(粗点线)

Figure 3b shows the T-H plot (solid curve). The throw increases from zero at the youngest layer 5 to a maximum at the oldest layer 0. The profile has a negative slope. The timing of initial faulting can be easily determined from the plot, where the throw is the largest.

The growth index (thick dotted curve in Figure 3b) also records the timing of faulting. The index is greater than 1.0 for all layers, which indicates the syn-faulting sedimentation in the hanging wall.

2.1.4 Comparison

Figure 4 compares the T-H plots of the three basic types of faults. The profiles are normalized by horizons along the vertical axis. The differences are obvious: a vertical profile characterizes the type I fault, a profile with a positive slope characterizes the type II fault, and a profile with a negative slope characterizes the type III fault. Implication in the curves is a clear timing indicator: all faults started after the horizon having the maximum throw was deposited. The analysis shows the fallacy of the common misconception that the maximum throw corresponds to the most active stage of faulting.

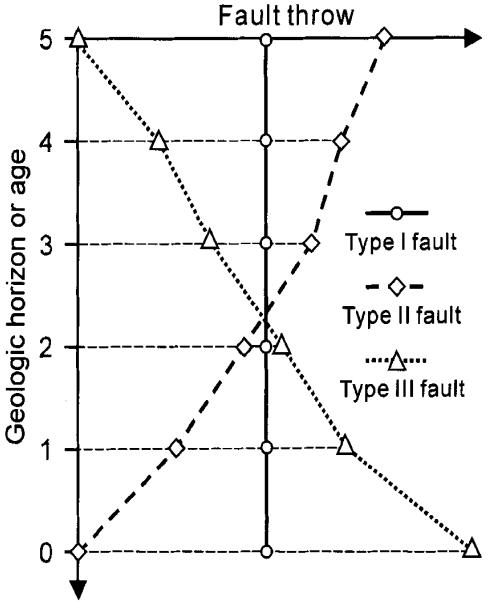

Fig. 4 Normalization and comparison of T-H plots of three basic types of normal faults

图4 三种基本正断层断距纵剖面的标准化及其比较图

Unfortunately, the exact time of fault initiation cannot be accurately determined for the type I and type II faults. There could be time hiatus between deposition of the youngest pre-faulting sediments and when faulting starts. Syn-faulting sediments are the key criteria to the timing determination.

2.2 Composite Models

The type I to type III models represent the simplest end-members. Faults with complex growth histories are more common in sedimentary basins. The following sections develop composite models that track changes in faulting styles and their throw profiles.

2.2.1 Composite post-and syn-depositional fault (type IC fault)

Figure 5a illustrates a schematic cross section through a fault with a combined kinematic history of the type I and type III faults, which is named type IC fault here. Faulting started after the prekinematic layers 0-3 were deposited and continued through deposition of the synkinematic layers 4 ~ 7.

The T-H plot (solid curve in Figure 5b) clearly indicates the kinematic history of the fault. Throws of the prekinematic layers 0 ~ 3 exhibit a vertical line as in the model type I fault (Figure 1b), whereas throws of the synkinematic layers 3 ~ 7 show a curve with a positive slope similar to that of the type III fault (Figure 2b). The maximum throw point on the throw profile marks the beginning of faulting.

The growth index (thick dotted curve in Figure 5b) also records the faulting timing and history, in which the growth index equals 1.0 for the prekinematic layers and is greater than 1.0 for the synkinematic layers.

2.2.2 Composite post-and syndepositional keystone fault (type IIC fault)

Figure 6a shows a schematic cross section through a fault having a combined kinematic history of the type II and type III faults, which is named type IIC fault here. In the section, layers 0 ~ 5 are prekinematic sediments and layers 6 ~ 9 are synkinematic sediments. The fault started as a keystone-stretching fault after the prekinematic layer 5 was deposited. It propagated downwards into the older prekinematic layers and grew upwards as the younger synkinematic layers were deposited.

Figure 6b shows the corresponding T-H plot (solid curve). In the prekinematic layers 1 ~ 5, fault throw is the largest at horizon 5 and decreases as the sedimentary layers become older. The throw is zero at the fault tip on horizon 1. This segment of the profile has a positive slope. In the synkinematic layers 6 ~ 9, the fault throw decreases as the sections become younger. The youngest horizon 9 is not faulted and has a zero throw. This segment of the throw profile has a negative slope. The resultant profile has a shape of combined type II and type III faults, which properly records the style and kinematic history of the fault. The throw maximum at the horizon 5 corresponds to the beginning of faulting.

The growth index (thick dotted curve in Figure 6b) correctly records the timing and growth history of the fault. However, it fails to differentiate it from the type IC fault.

For an embedded fault, here defined as a postdepositional fault that is fully contained within a

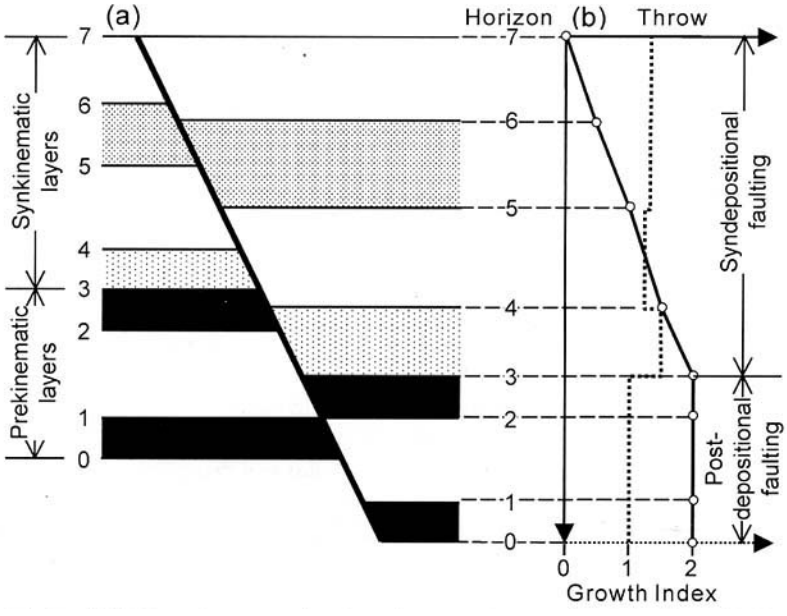

Fig. 5　(a) Schematic cross section through a composite normal fault that has a simple postdepositional and (b) T-H plot (thick solid line) and growth index plot (thick dotted curve)

图 5　(a)简单后沉积与同沉积复合型正断层剖面示意图
及其(b)断距纵部面图(粗实线)和断层生长指数图(粗点线)

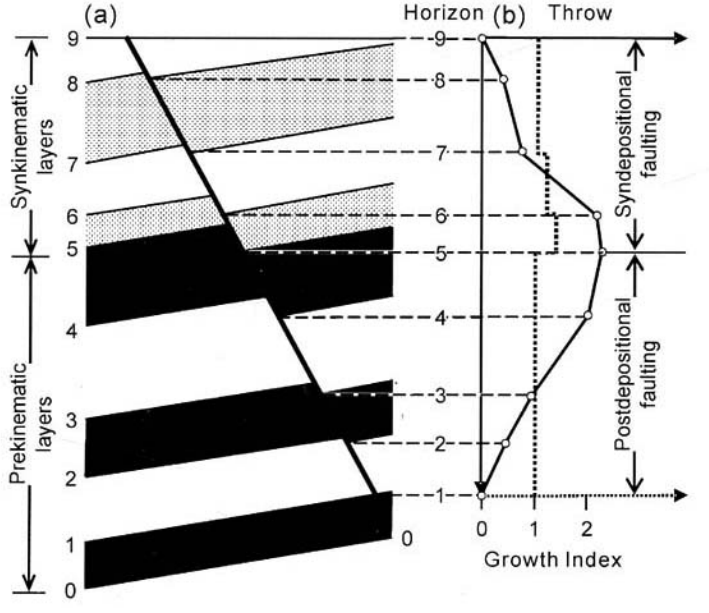

Fig. 6　(a) Schematic cross section through a composite normal fault that has apostdepositional keystone-stretching and (b) T-H plot (thick solid line) and growth index plot (thick dotted curve)

图 6　(a)后沉积拱顶拉伸与同沉积复合型正断层剖面示意图
及其(b)断距纵部面图(粗实线)和断层生长指数图(粗点线)

sedimentary package, throw typically increases from zero at the upper tip to a maximum and then decreases to zero at the lower tip (e. g., Barnett et al, 1987; Walsh and Watterson, 1988). The throw profile thus is identical to that of a type IIC fault. The stratigraphic analysis and growth index plot should differentiate them.

2.2.3 Episodic normal growth fault

Episodic normal faulting is common in basin evolution history (e. g., Etheridge, 1986; McLaurin and Burleigh, 2001). A fault could be buried by sediments during tectonically quiet episodes and then rejuvenated by subsequent faulting. A possible stacking pattern of such a fault is schematically illustrated in Figure 7a. The fault was active during the depositional intervals of 0~2, 6~9, and 12~14, which is indicated by the expanded sediments in the hanging wall. The fault was dormant and buried during the deposition of intervals of 2~6 and 9~12, which is indicated by the constant thickness of intervals across the fault.

Figure 7b shows the T-H plot. The profile shows a curve with alternating vertical and sloped segments. The sloped segments have positive slope and mark the active periods of syndepositional faulting. The vertical segments mark the burial and dormant periods. The maximum throw point at layer 0 marks the timing of the initial faulting. Where the profile changes from a sloped curve to a vertical line (e. g., bends at horizons 2 and 9), the fault became inactive and was buried. Where the profile changes from a vertical line to a sloped curve (e. g., bends at horizons 6 and 12), the fault rejuvenated.

The growth index plot (thick dotted curve in Figure 7b) also well depicts the episodic growth (index > 1.0) and burial (index = 1.0) history of the fault.

2.2.4 Inverted normal growth fault

Figure 8a shows a schematic cross section through

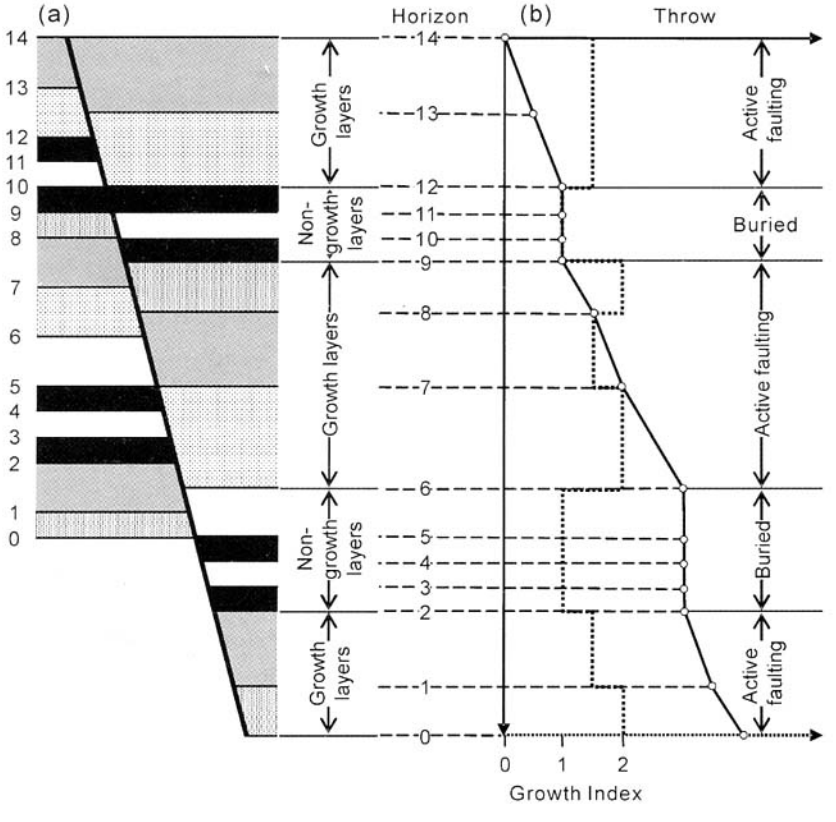

Fig. 7 (a) Schematic cross section through a normal fault that has multiple episodes of burial and (b) T-H plot (thick solid line) and growth index plot (thick dotted line)

图7 (a)多期活动与掩埋的生长正断层剖面示意图
及其(b)断距纵部面图(粗实线)和断层生长指数图(粗点线)

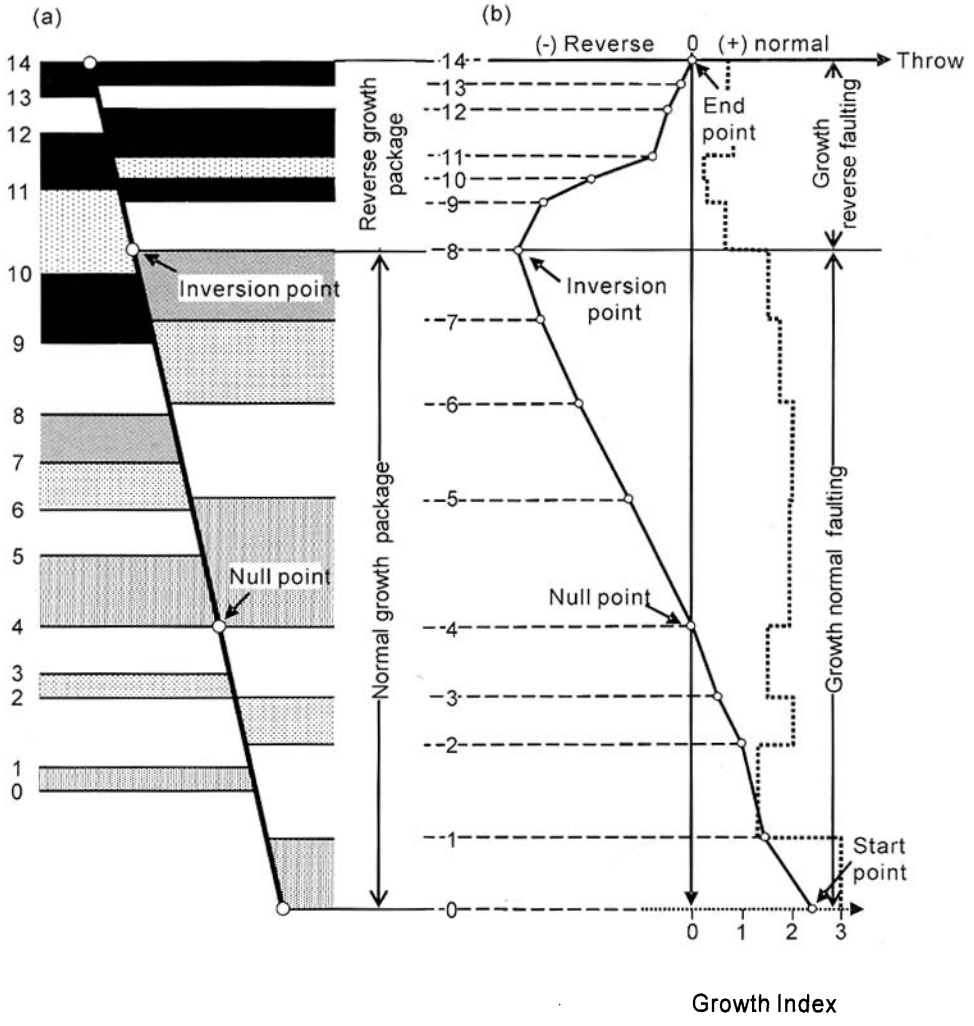

Fig. 8　(a) Schematic cross section through an inverted normal growth fault and (b) T-H plot (thick solid line) and growth index plot (thick dotted line)

图 8　(a)逆转生长正断层剖面示意图
及其(b)断距纵部面图(粗实线)和断层生长指数图(粗点线)

an inverted growth fault. The fault was a normal growth fault during the deposition of layers 1 ~ 8. It was then inverted to a reverse fault during the deposition of layers 9 ~ 14.

Figure 8b shows the T-H plot. The reverse throws are plotted as negative values. The plot is marked by four key points: a start point, a null point, an inversion point, and an end point. The start point has a maximum throw and marks the beginning of initial normal faulting. The null point has zero throw along the fault, where the horizon has no apparent offset. The inversion point (deflection point) has a minimum throw (or a maximum reverse throw), which marks the beginning of the inversion. The end point has zero throw and marks the end of faulting. The profile has a negative slope between the inversion and start points. The profile has a positive slope between the inversion and end points.

The growth index plot (thick dotted curve in Figure 8b) also differentiates the normal growth episode (where the index > 1.0) from the reverse growth episode (where index < 1.0). However, it fails to locate the null point.

2.3 Geologic Influences on Profile Geometry

During our analysis of geological faults, we encountered some profiles whose shapes were deviated from the basic and composite models. The profiles could not be simply explained by different fault types. Other geological factors must have caused the deviations. We initially investigated the influences of compaction, erosion, and near-fault deformation on the shapes of profiles. Our analysis suggested that compaction and erosion have little impact, thus are omitted here. Only the effects of near-fault drags are presented.

2.3.1 Effect of normal drag in hanging wall

Figure 9A-a shows the normal drag of horizons 4 and 5 in the hanging wall of a normal growth fault. Other layers are not affected. The drag effectively reduces the true throw between the cutoffs of the equivalent horizons across the fault. The local decrease of the throw creates a dent in the profile (thick solid curve in Figure 9A-b), when compared with the profile (thick dashed curve in Figure 9A-b) without the drag effect. However, the overall geometry of the profile resembles that of the type III fault.

2.3.2 Effect of reverse or rollover drag in hanging wall

In Figure 9B-a, layers 5 and 6 in the hanging wall of a normal growth fault form reverse or rollover drag. Oher layers are not involved. The reverse drag effectively increases the fault throw. The local throw increase on horizons 5 and 6 creates a bump in the profile (thick solid curve in Figure 9B-b), which otherwise would be a typical type III fault throw profile (thick dashed curve in Figure 9B-b).

2.3.3 Effect of normal drag in footwall

Figure 10A-a schematically shows a cross section through a normal growth fault. The footwall layers 4 and 5 are bent by normal drag into the fault. Other layers are not affected. The drag reduces the true throw, which creates a dent in the profile (solid curve in Figure 10A-b), when compared with the profile without drag effects (thick dashed curve in Figure 10A-b).

2.3.4 Effect of reverse drag in footwall

Figure 10B-a schematically shows a cross section through a normal growth fault. The footwall layers 4 and 5 are dragged upward against the fault. The drag increases the apparent throw. Accordingly, a bump in the fault throw profile records the drag-induced throw increase (solid curve in Figure 10B-b).

3 Geologic Examples

This section applies conceptual models to the normal faults in the Peng Lai 19-3 Oil Field in the Bohai Bay basin, offshore China. The overall structure of the field is an anticline within the Tancheng-Lujiang (Tan-Lu) fault zone (O'Reilly et al, 2000). Both right-lateral wrenching of the Tan-Lu fault zone and bending of the cover sediments above the pre-Tertiary basement uplift formed the anticline. The anticline is intersected by three nearly NS-trending strike-slip fault zones and by numerous NE-trending normal faults (Figure 11). The strike-slip faults are part of the regional Tan-Lu system and are segmented along the strike. The normal faults divide the anticline into a series of horsts and grabens. The bounding faults of the grabens show en echelon arrangement.

Nine faults from three time-migrated seismic lines are presented. They are from five fault zones in the north and west of the field (Figure 11). All the selected faults cut or terminate near the top of the Oligocene Dongying Formation and tip out in the shallow Quaternary sediments.

Figure 12a is a seismic profile across faults F1, F2, and F3. Horizon H0 is the top of the Oligocene Dongying Fm. Horizon H2 is near the top of the Miocene Guantao Fm. Horizon H6 is near the top of the Pliocene Minghuazhen Fm. Horizons H1 and H3 are near the base and near the top of the oil-bearing reservoir, respectively. The bright reflector below H0 is the top of the pre-Tertiary basement. Horizons H0 through H6 were fully correlated in a 3-dimensional seismic data. Horizons H7 through H10 were only correlated locally to increase the plot point density; they may not be the same horizons from section to section.

Figure 12b shows the T-H plots of faults F1, F2, and F3. Faults F1 and F3 seem to have relatively simple fault throw profiles. Fault F1 increases in throw from zero within the shallow Quaternary section to a maximum at about horizon H4 and then decreases to zero at horizon H0, which is a typical type IIC fault throw profile. Although there are rollover drags between horizons H1 through H6 in the hanging wall, they dont seem to be the local isolated effects. Apparent local reverse drags occur between horizons H3 to H5 in the footwall and create a minor bump in the profile. The adjusted profile (dashed curve) after the removal of the drag-effected throw remains similar to its original one. Fault F3 has a similar throw profile to that of fault F1.

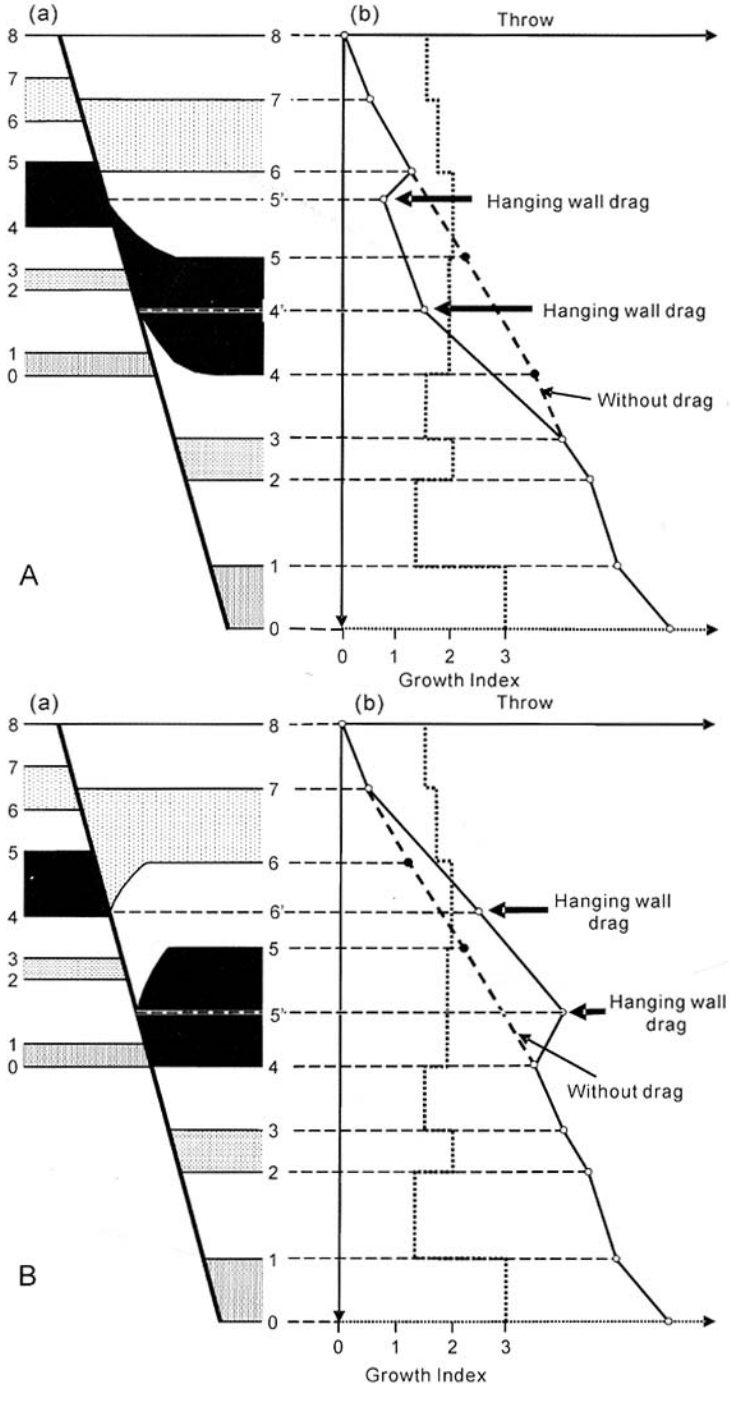

(a) Schematic cross section through fault; (b) T-H plot (thick solid curve) and growth index plot (thick dotted curve)
(a)生长正断层剖面示意图及其(b)断距纵剖面图(粗实线)和断层生长指数图(粗点线)

Fig. 9　Effect of local normal drag (A) and reverse drag(B) in hanging wall on geometry of fault throw profile
图 9　断层上盘局部正拖曳(A)和逆拖曳(B)对断距纵剖面形态影响.

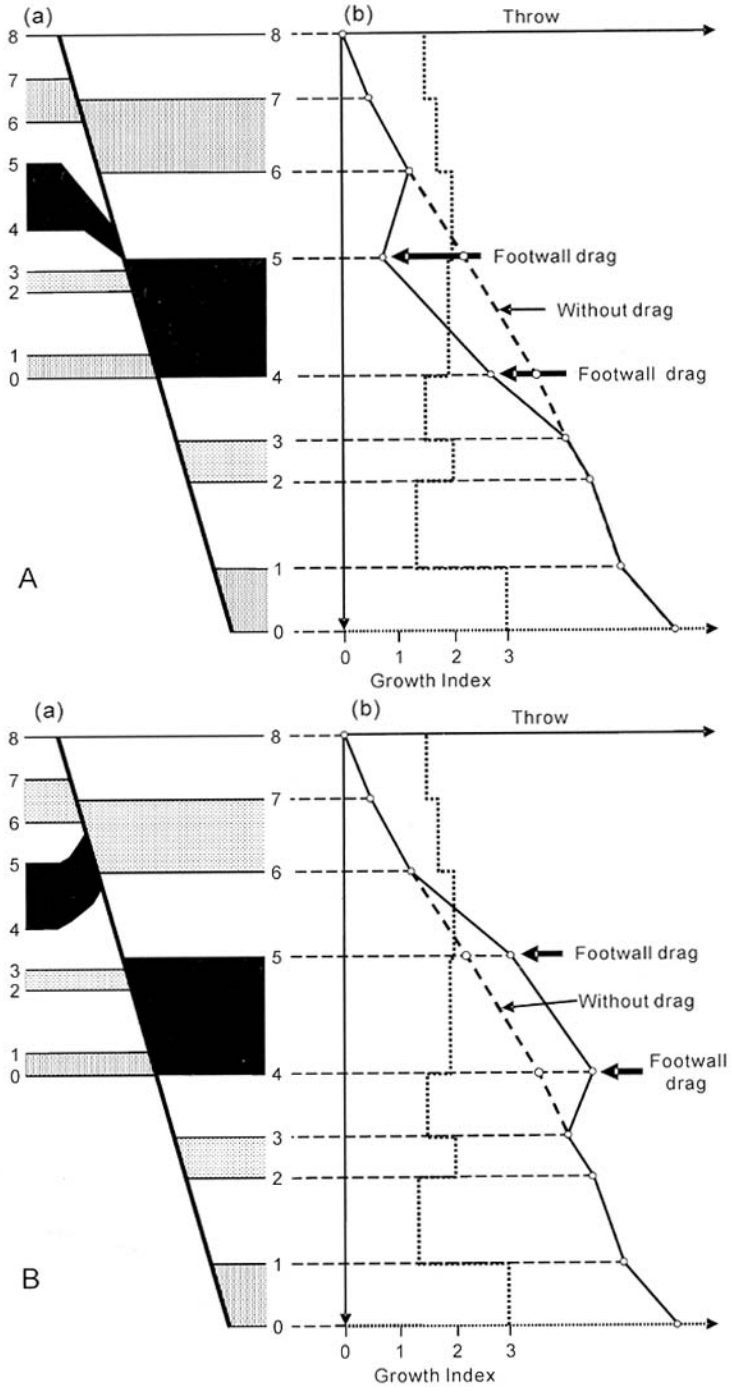

(a) Schematic cross section through fault; (b) T-H plot (thick solid curve) and growth index plot (thick dotted curve)
(a)生长正断层剖面示意图;(b)断距纵剖面图(粗实线)和断层生长指数图(粗点线)

Fig. 10 Effect of local drag (A) and reverse drag (B) in footwall on geometry of fault throw profile.

图 10 断层下盘局部正拖曳(A)和逆拖曳(B)对断距纵剖面形态影响

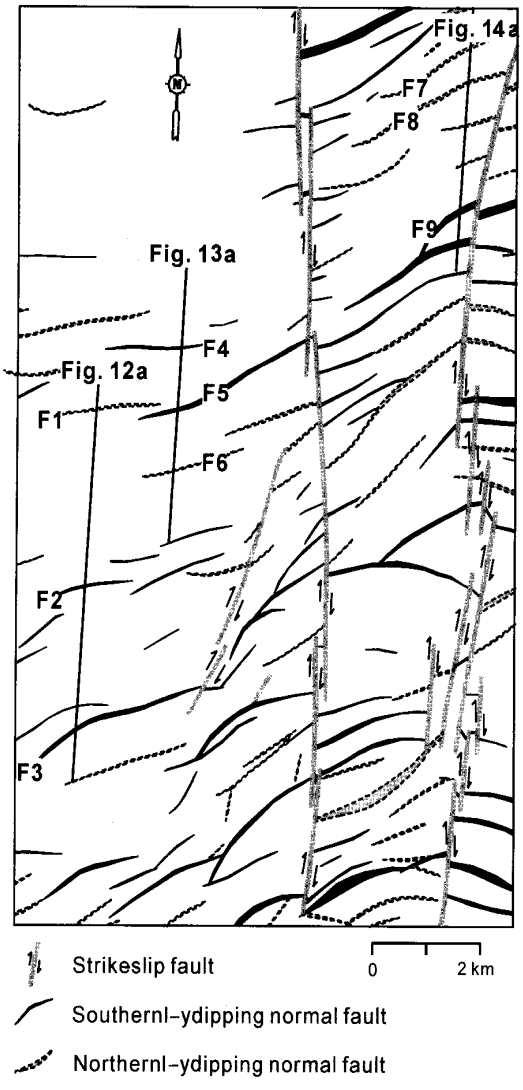

Fig. 11　Fault map on near top reservoir horizon on Peng Lai 19-3 Oil Field

图 11　蓬莱 19-3 油田近储层顶面断层分布图

Throw increases from zero within the shallow Quaternary sediments to a maximum at about horizon H4 and then decreases to zero at horizon H0. Both profiles suggest that faults F1 and F3 started as a keystone-stretching fault after horizon H4 was deposited. Sections between H0 and H4 are pre-faulting, non-growth sediments. Sediments between H4 and upper tips of faults are growth strata.

The throw profile of fault F2 has a rather irregular shape. A dent and two bumps occur in the profile. The throw increases from zero at the upper fault tip to a local maximum around H6. It then decreases to H4 followed by an increase to a maximum around H2, which is followed by another decrease. Normal drags of horizons H1 through H3 in the hanging wall probably have increased the apparent throws. However, the dent in the middle of the profile remains even after the local effects are roughly corrected (dashed line). A closer examination shows that the section between H4 and H5 in the hanging wall is thinner than in the footwall, suggesting the possible mis-ties of the autopicked horizon H4. The timing of faulting thus could not be accurately determined from the current profile.

The growth index plot (solid red curve in Figure 12b) for fault F1 supports the profile interpretation. The index from horizons H0 to H4 is about 1.0, indicating that they are the pre-faulting sedimentary package. The index between the upper tip of the fault and horizon H4 is generally greater than 1.0, indicating the growth episode of the fault. The index of layer 10 (between horizons H9 and H10) is about 1.0, suggesting a burial episode of the fault. The burial episode is also documented by the throw profiles, where the segments are nearly vertical.

Figure 13a is a seismic line across faults F4, F5, and F6. All three faults are from the same fault zone

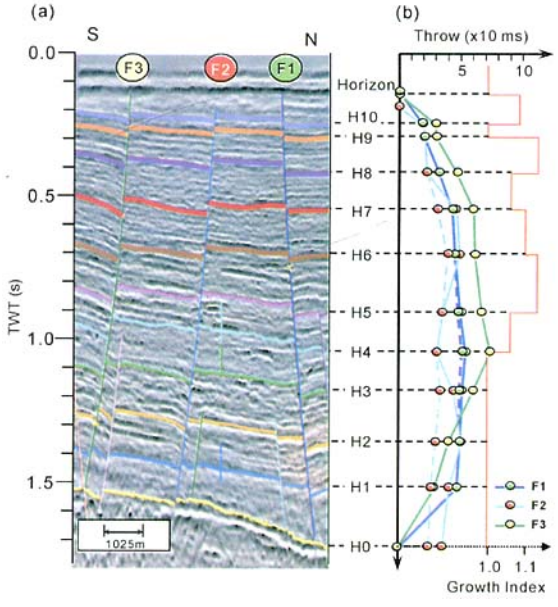

Fig. 12　(a) Seismic section through faults F1, F2, and F3 in western flank of Peng Lai 19-3 Oil Field; (b) T-H plots for faults F1, F2, and F3. The growth index for fault F1 is plotted as a red curve in Figure 14b.

图 12　(a)蓬莱 19-3 油田西翼穿过断层 F1, F2, F3 的地震剖面图及(b)断距纵剖面图和断层 F1 的生长指数图(红折线)

(Figure 11). Figure 13b shows their T-H plots. All faults have a type IIC profile. Faults F4 and F6 increase in throw from zero in the shallow Quaternary sediments to a maximum near H1 and then rapidly decrease to zero near horizon H0, suggesting that both faults initiated around the deposition of horizon H1. Sediments between H1 and upper tips of faults thus are a syn-faulting package. The throw profile of fault F5 has an apparent type IIC fault throw profile geometry. The profile shape is affected by reverse (rollover) drag in the hanging wall, which creates a bump in the middle of the profile. The profile suggests that fault F5 initiated around the deposition of horizon H4 by crestal stretching.

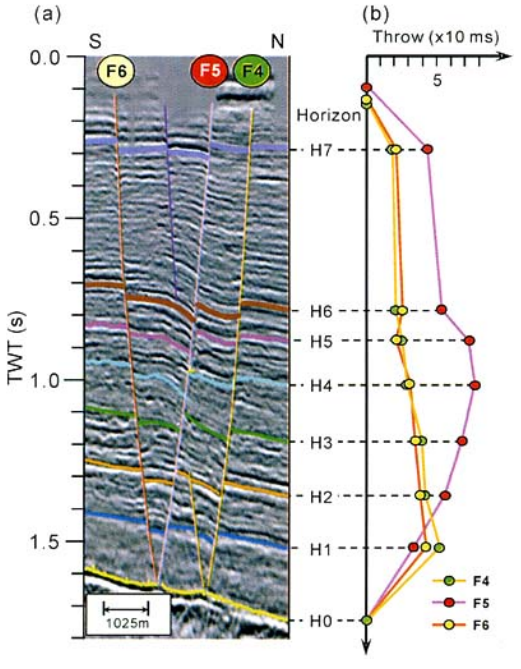

Fig. 13 (a) Seismic section through faults F4, F5, and F6 in western flank of Peng Lai 19-3 Oil Field. (b) T-H plots for faults F4, F5, and F6

图13 (a)蓬莱19-3油田西翼穿过断层F4, F5, F6的地震剖面图及(b)断距纵剖面图和断距纵剖面图

Figure 14a is a seismic profile through faults F7, F8, and F9. Faults are from two fault zones (Figure 11). Interpretations of their T-H plots (Figure 14b) are rather straightforward. Although minor bumps and dents occur in the profile of fault F8, throw generally increases from zero at the upper tip of the faults to a maximum, followed by decreases, resulting in typical type IIC fault throw profiles. The bumps seem to be the result of rollover drag between horizons H7 through H9 in the hanging wall of fault 8. The profiles suggest that faults F7 and F8 initiated around the deposition of H1 and fault F9 started at around H4, which are consistent with the other faults.

4 Conclusions

(1) Fault throw profile (T-H plot) plots cumulative fault throw versus stratigraphic horizon or geologic age from a geo-section. The technique provides a simple but rather robust graphical method to assess the styles, tim ing of initiation, and kinematic history of normal and simply inverted normal faults.

(2) The conceptual models of the throw profiles unambiguously distinguish three basic types of normal faults and their timing of initiation. A profile with a vertical line segment indicates a simple postdepositional fault. The top of the line segment corresponds to the earliest possible timing of fault initiation. A profile in which fault throw decreases with the increase of horizon age from a maximum to zero indicates a postdepositional keystone-stretching fault. The throw maximum corresponds to the earliest possible timing of the fault initiation. A profile in which fault throw increases with the increase of horizon age indicates a simple syndepositional growth fault. The throw maximum corresponds to the start timing of the fault.

(3) For a composite normal fault, major inflections in the T-H plot indicate the changes of the fault styles. Change of the profile from a vertical line to a curve of a negative slope marks the change from a simple postdepositional fault to a growth fault. Repeated stacking of this type of profile indicates multiple episodes of growth and burial of a normal fault. Change of the profile slope from positive to negative marks the change from a postdepositional keystone-stretching fault to a growth fault. The T-H plot of an inverted normal growth fault is characterized by four key points: a start point, a null point, an inversion point, and an end point.

(4) The conceptual models show that local drags have the largest impact on the profile geometry. Normal drags in either hanging wall or footwall create dents, whereas reverse drags create bumps in the profiles.

Acknowledgements We thank Tian Lixin (China National Offshore Oil Company) for the constructive discussions and comments on both the conceptual models and general geology of the Peng Lai 19-3 Oil

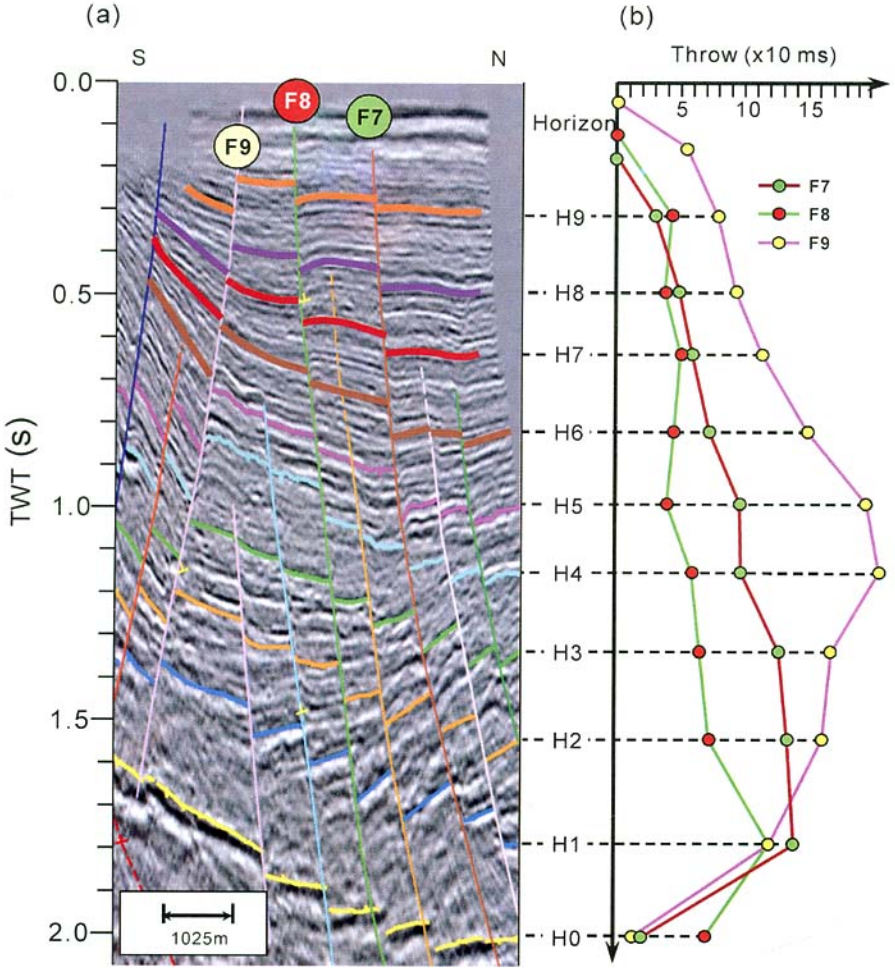

Fig. 14　(a) Seismic section through faults F7, F8, and F9 in western flank of Peng Lai 19-3 Oil Field. (b) T-H plots for faults F4, F5, and F6

图 14　(a)蓬莱 19-3 油田西翼穿过断层 F7, F8, F9 的地震剖面图及(b)断距纵剖面图

Field. Scot Krueger and Joseph Devay (both ConocoPhillips) critically reviewed and greatly improved earlier versions of the manuscript.

References:

Allan U S. **1989**. Model for hydrocarbon migration and entrapment within faulted structures. ***AAPG Bulletin***, 73(7): 803 - 811.

Barnett J A M, Mortimer J, Rippon J H, et al. **1987**. Displacement geometry in the volume containing a single normal fault. ***AAPG Bulletin***, 71(8): 925 - 937.

Beach A and Trayner P. **1991**. The geometry of normal faults in a sector of the offshore Nile Delta, Egypt. In: Roberts A M, Yielding G and Freeman B, eds. The Geometry of Normal Faults. ***Geological Society (London) Special Publication***, 56: 173 - 182.

Bischke R E. **1994**. Interpreting sedimentary growth structures from well log and seismic data (with examples). ***AAPG Bulletin***, 78(6): 873 - 892.

Chapman T J and Meneilly A W. **1991**. The displacement patterns associated with a reverse - reactivated, normal growth fault. In: Roberts A M, Yielding G and Freeman B, eds. The Geometry of Normal Faults. ***Geological Society (London) Special Publication***, 56: 183 - 191.

Davis R K, Medwedeff D A, G. P. O'Donnell G P, et al. **1996**.

Regional and reservoir-scale analysis of fault systems and structural development of Pagerungan gas field, East Java Sea, Indonesia (abs). ***AAPG Annual Convention Program***, 5: A33.

Demaison G and Huizinga B J. **1991**. Genetic classifications of petroleum systems. ***AAPG Bulletin***, 75(10):1626-1643.

Derer C, Kosinowski C M, Luterbacher H P, et al. **2003**. Sedimentary response to tectonics in extensional basins: the Pechelbronn Beds (late Eocene to early Oligocene) in the northern Upper Rhine Graben, Germany. In: McCann T and A. Saintot A, eds. Tracing Tectonic Deformation Using the Sediment Record. ***Geological Society (London) Special Publications***, 208: 55-69.

Etheridge M A. **1986**. On the reactivation of extensional fault systems. ***Philosophical Transactions of the Royal Society of London***, 317: 179-194.

Ge Hongxing and Vendeville B C. **1994**. The origin of the Dongzhuang rollover structure ? an insight from scaled physical experiments, ***Acta Petrolei Sinica***, 15(1): 17-25.

Hardman R F P and Booth J E. **1991**. The significance of normal faults in the exploration and production of North Sea hydrocarbons. In: A. M. Roberts A M, Yielding G and Freeman B, eds. The Geometry of Normal Faults. ***Geological Society (London) Special Publication***, 56: 1-13.

Link T A. **1930**. Experiments relating to salt-dome structures. ***AAPG Bulletin***, 14(4): 483-508.

McClay K R and Ellis P G. **1987**. Analogue models of extensional fault geometries. In: Coward M P, Dewey J F and Hancock P L, eds. Continental Extensional Tectonics. ***Geological Society (London) Special Publication***, 28: 109-125.

McLaurin B T and Burleigh H W. **2001**. Paleocene faulting within the Beaufort Group, Atlantic Coastal Plain, North Carolina. ***GSA Bulletin***, 113(5): 591-603.

Morley C K. **2002**. Evolution of large normal faults: evidence from seismic refection data. ***AAPG Bulletin***, 86(6): 961-978.

Nunns A G. **1991**. Structural restoration of seismic and geologic sections in extensional regimes. ***AAPG Bulletin***, 75(2): 278-297.

O'Reilly J B, Ge Hongxing, Sharrah K, et al. **2000**. Fault geometry and kinematics in the Peng Lai 19-3 field, Bohai Bay, People's Republic of China (abs). ***AAPG Bulletin***, 84 (9): 1472.

Peacock D C P and Sanderson D J. **1991**. Displacements, segment linkage and relay ramps in normal fault zones. ***Journal of Structural Geology***, 13(6): 721-733.

Rowan M G and Kligfield R. **1989**. Cross section restoration and balancing as aid to seismic interpretation in extensional terranes. ***AAPG Bulletin***, 73(8): 955-966.

Schultz-Ela D D. **1992**. Restoration of cross-sections to constrain deformation processes of extensional terranes. ***Marine and Petroleum Geology***, 9(4):372-388.

Tearpock D and Bischke R E. **1991**. Applied subsurface geological mapping. ***New York: Prentice-Hall***, 648 p.

Walsh J J and Watterson J. **1988**. Analysis of the relationship between displacement and dimensions of faults. ***Journal of Structural Geology***, 10(3): 239-247.

Walsh J J and Watterson J. **1991**. Geometric and kinematic coherence and scale effects in normal fault system. In: Roberts A M, Yielding G and Freeman B, eds. The Geometry of Normal Faults. ***Geological Society (London) Special Publication***, 56: 193-203.

Watterson J. **1986**. Fault dimensions, displacements and growth. ***Pure and Applied Geophysics***, 124(1-2): 365-373.

Williams G D, Powell C M and Cooper M A. **1989**. Geometry and kinematics of inversion tectonics. In: Cooper M A and Williams G D, eds. Inversion Tectonics. ***Geological Society (London) Special Publication***, 44: 3-15.

Worrall D M and Snelson S. **1989**. Evolution of the northern Gulf of Mexico, with emphasis on Cenozoic growth faulting and the role of salt. In: Bally A W and Palmer A R, eds. The Geology of North America: An Overview. Boulder, Colorado: Geological Society of America, A: 97-138.